https://doi.org/10.5194/angeo-2020-68
Preprint. Discussion started: 17 February 2021

Annales Geophysicae Discussions

Simulation of Gravity Wave D-region disturbance and its effect on the LWPC simulated VLF signal.

Abdellatif Benchafaa[1] , Samir Nait Amor[2] , Ghazali Mebarki[3]

[1] Department of physic, Faculty of science, University of Batna1, Algeria

[2] Center for Research in Astronomy Astrophysics and Geophysics, Algeria

[3] LESEI Laboratory, Department of Mechanical engineering, Faculty of Technology, University of Batna 2, Algeria

Correspondence to: Benchafaa Abdellatif (benchafaaa@yahoo.com)

Abstract

In this work we show the result of the numerical simulation of the gravity waves (GWs) D region disturbance. Effectively, using the Glukhov-Pasko-Inan (GPI) model of the electron density in the D region we were figured out the response of the electron density due to gravity wave neutral atmosphere oscillation. As a consequence to the D region disturbance, the electron density sometimes increases when the neutral atmosphere density decreases and vice versa. This behavior was interpreted by the decreases or increases of ionization rate by chemical loss process. In a second simulation work, we used the Long Wave Propagation Capability (LWPC) code to simulate the Very Low Frequency (VLF) signal when the gravity wave disturbance crossed the VLF path. The effect of the disturbance is to decrease the VLF signal reflection height below the ambient altitude (87 km) when the electron density increases. On the other hand and when the electron density drops, the VLF reflection altitude increased higher than 87 km.

1 Introduction

The lower layer of the ionosphere, known as the D region, with the Earth surface constitute the Earth-Ionospheric Wave guide (EIWG) that allows the propagation of the electromagnetic wave signal in the range of VLF-LF frequencies. Therefore, any modification in the D region composition (mainly the electron density) can appear as a perturbation in the VLF signal. The D region disturbances are of different sources such as: solar flares, solar energetic particles, thunderstorm activity… Several works were done in order to characterize the signal amplitude perturbations caused by to the D region disturbances. Indeed, the solar flares effect on the propagation of the VLF signal was widely studied and thus the connection between the increases in the D region electron density with the increases of the solar flares power was established (Raulin et al., 2013; Kumar et al., 2015). In another work and by the use of two separate VLF receiver locations data, NaitAmor et al (2010) showed the role of the geometry on the Early VLF signal perturbation properties associated with thunderstorm activity in the Mediterranean Sea. Using the LWPC code, NaitAmor et al (2016) simulated the Early VLF signal perturbations due to a gigantic jet and elve observed in the Mediterranean Sea (Vander Veld et al., 2010) where they found that the increase of the D region electron density below 87 km causes the reflection of the VLF signal at lower altitudes. In recent years, people are attracted by the effect of the natural phenomena known as Acoustic and Gravity Waves (AGWs) on the propagation of the VLF signal. The AGWs are disturbances of the Earth neutral atmosphere that can propagate to higher altitudes. Several natural disturbance sources can generate AGWs like Earthquake, tsunamis, cyclone… Different observation tools were developed and used to study the AGWs disturbances that include the ground-based observations of atmospheric infrasound (Le Pichon et al., 2010), radar data (Dhaka et al., 74 2003), GPS occultation data (Ming et al., 2014; Perevalova and Ishin., 2011; Song et al., 2017). In addition to the instrumental works, numerical simulations on the propagation of the AGWs in the atmosphere and ionosphere were done (Graves et al., 1996; Ding et al., 2003; Brissaud et al., 2016; Occhipinti et al., 2011; Marshall and Snively, 2014).

The use of the Very Low Frequency signal (VLF) sounding constitutes a powerful technique to study the effect of the AGWs on the mesosphere and lower thermosphere, between 80 km and 100 km, and the D region. Effectively, the narrowband VLF signal amplitude (NB-VLF) data were used to determine the wave period of the AGWs generated by: day/night terminator (Pal et al., 2015),

https://doi.org/10.5194/angeo-2020-68
Preprint. Discussion started: 17 February 2021

Annales Geophysicae Discussions
Open Access
EGU

meteorological systems (Rozhnoi et al., 2014; Nina and Cadez, 2013; Kumar et al., 2017; NaitAmor et al., 2018), thunderstorms (Marshall and Snively, 2014) and tsunami (Rozhnoi et al., 2014). In these works, a clear evidence of the AGWs disturbances was observed in the VLF signal amplitude. Additionally, the wavelet analysis of the signal amplitude revealed a wave period from 10 s to 3 hours depending on the AGW sources. In another work, Kumar et al (2017) used the LWPC code to simulate the perturbed VLF signal amplitude and phase due to tropical cyclone Evan in the south pacific region. Their results showed that the reference height of the Wait parameter decreased by 5.1 km from its ambient value (87 km). In this work, we present a simulation results about the effect of the AGWs on the electron density of the D region of the ionosphere and VLF signal. In section 2, we describe the simulation method and the set of continuity equations of charged particles known as Glukhov-Pasko-Inan (GPI) model to get the electron density variation in the D region. Then, in section 3 we present the method to simulate the VLF signal amplitude using LWPC code and the GPI simulation results. Finally, section 4 we show and discus our simulation result.

2 Description of the method

To simulate the disturbance of the lower ionosphere due to the GW-neutral atmosphere interaction, we suppose that the neutral atmospheric density follows the function given in Eq. (1). This distribution function was used to describe the bottom pumping momentum of the gravity wave that propagates in the atmosphere. The function has two spatial dimensions (x, z) for simplicity and that for our case x varies from 0 to 2000 km and in the z direction it varies from 80 km to 90 km.

$$N(x,z,t) = N_0 \exp\left(\frac{(x-x_c)^2}{2\sigma_x^2}\right) \exp\left(\frac{(z-z_c)^2}{2\sigma_z^2}\right) \exp\left(\frac{(t-t_c)^2}{2\sigma_t^2}\right) \cos(\omega t) \quad (1)$$

Where: $\sigma_x = 200$ km, $\sigma_z = 10$ km, $\sigma_t = 4000$ s and N_0 is the ambient neutral density at each altitude taken from MSIS (Hedin, 1991). Additionally, we suppose that the disturbance moves in the x direction at a wind speed of 50 m/s as shown in Fig. 1(a). In the z direction the speed was supposed to be 10 km/s. The spatial integration steps (x, z) are (50 km, 1 km) and for time integration the step is 0.5 s. The time reference (i.e. t=00:00:00) corresponds to the time when the disturbance center reaches the crossing location between the x axis and y axis (Figure 1(a)). The spatio-temporal profile of the neutral density is shown in Fig. 1(b and c) where it is a Gaussian in the x direction and as function of time is exponentially damped shape. In our simulation the neutral density of the atmosphere is just a parameter to be introduced in the GPI model of the charged particle continuity equations. Thus, the neutral profile given in Eq. (1) can be changed depending on the neutral atmosphere disturbance source.

To describe the lower ionosphere region (the D region) chemistry, Glukhov-Pasko-Inan (1992) proposed a set of four continuity equations of the charged particles based on the equilibrium between the production and loss rates of particles dues to different chemical process. This model was thereafter known as GPI model of the D region of the ionosphere. The model is represented by equations (2) to (5) and closed with the neutrality equation of charged particles $N_e + N^- = N^+ + N_x^+$. Here N_e denotes the electrons density, N^+ represents the positive ions density, N^- is the negative ions density and finally N_x^+ denotes the positive cluster ions density.

$$\frac{dN_e}{dt} = q + \gamma N^- - \beta N_e - \alpha_d N_e N^+ - \alpha_d^c N_e N_x^+ \quad (2)$$

$$\frac{dN^-}{dt} = \beta N_e - \gamma N^- - \alpha_i N^- \quad (3)$$

$$\frac{dN^+}{dt} = q - BN^- - \alpha_d N_e N^+ - \alpha_i N^- N^+ \quad (4)$$

$$\frac{dN_x^+}{dt} = BN^+ - \alpha_d^c N_e N_x^+ - \alpha_i N^- N_x^+ \quad (5)$$

Since we are studying the nighttime ionosphere, the q parameter represents the electron production term due to cosmic rays taken from (Velinov et al., 2013). β is the electron attachment rate, γ the electron detachment rate, α_d is the coefficient of dissociative recombination, α_d^c is the effective coefficient of recombination of electrons with positive cluster ions, α_i is the coefficient of ion-ion

https://doi.org/10.5194/angeo-2020-68
Preprint. Discussion started: 17 February 2021

Annales Geophysicae Discussions

recombination (mutual neutralization) for all kinds of positive ions with negative ions and B is the rate of conversion of positive ions into positive cluster ions. In our case, the used parameters are given by the expressions:

$$\gamma = 3 \times 10^{-18} N(s^{-1}),$$

$$\alpha_d = 3 \times 10^{-7} (cm^3 s^{-1}),$$

$$\alpha_d^c = 10^{-5} (cm^3 s^{-1}),$$

$$\alpha_i = 10^{-7} (cm^3 s^{-1}),$$

$$B = 10^{-31} N^2 (s^{-1}),$$

$$\beta = 10^{-31} N_{O_2} N_{N_2} + 1{,}4 \times 10^{-29} \left(\frac{300}{T}\right) e^{\frac{-600}{T}} N_{O_2}^2 (s^{-1})$$

Here, N_{O_2} and N_{N_2} represent the number densities of neutral molecular oxygen and nitrogen expressed in cm^{-3}, whereas T is the electron temperature. More information about the model and mathematical formalism can be found in (Glukhov et al., 1992).

The GPI model was used to describe the response of the D region to different source of perturbations like solar flares (Palit et al., 2014), energetic electron precipitations (LEP) (Glukhov et al., 1992; Inan et al., 2010) lightning electric field (Haldoupis et al., 2009)… Unlike the studies cited above where the neutral atmosphere is assumed to be constant and only varies with altitude; the neutral atmosphere in our study is considered as a space and time varying parameter. The aim of this simulation is to show the effect of the neutral atmosphere disturbance on the D region ionization and hence the VLF signal propagation. This later is simulated using the LWPC code (Ferguson, 1998). The code uses the Wait and Spies electron density profile which depends on two parameters: the reference height H' (in km) and the sharpness factor β (in km^{-1}) (Wait and Spies, 1964)**.** In the ambient nighttime ionosphere, these parameters are latitude and frequency dependence and that at the mid-latitude regions H' equals 87 km. Several works using the LWPC code have been devoted to determine the electron density changes dues to solar flares (Palit et al., 2014), Early/Fast events (NaitAmor et al., 2016), electron precipitations (Glukhov et al., 1992), meteorological convective systems (Kumar et al., 2017). In these works, the authors searched the modified values of H' and β that lead to a simulated signal amplitude and phase close to the measured ones. In our case, the reference height H' is obtained from the GPI numerical results when the simulated electron density at a given altitude, n_e (z), equals the ambient one at 87 km i.e. n_e (z) = 30.74 cm^{-3}. This new altitude is then considered as the new reference height that we used in the LWPC code. Repeating this operation several times, we obtain the time variation of the signal amplitude and phase at each location between the transmitter and the receiver. For geometry purpose, we supposed that the VLF signal propagates between the transmitter and the receiver along the y axis, see Fig. 1(a).

3 Numerical Results

The aim of this study is to find by numerical simulation when and where the electron density becomes equal the ambient one given by LWPC code (30.74 cm^{-3}) for z = H'= 87 km. An example of time-dependent profile of the electron density obtained numerically at z = 85 km and at three different positions x is shown in Fig. 2(b). Since we have assumed a totally neutral atmosphere, we can notice that the electron density increases to a saturation value which results from the equilibrium between the production of pair (electron-ion) and the loss terms. After that and when the neutral atmosphere disturbance arrives, the electron density shows opposite behavior compared to the neutral species where it increases when the neutral density decreases and vice-versa. This is due to the rupture of the balance between the production of pair (electron-ion) and the loss terms. Indeed, when the disturbance pushes the neutral species upward, the loss terms (recombination and attachment) increase leading to reduction of the electron density number. In the other side, when the disturbance pushes the neutrals species downward, the loss terms decrease and thus the electron density production increases. These effects appear at all altitudes and at any position on the x axis so the only difference is on the level of the modified electron density. Therefore, when the disturbance reaches to the sensitive zone of the VLF Great Circle Path (GCP) or crosses it, the reflection altitude of the VLF signal changes and may increases or decreases. This modification of the GCP appears as perturbations

https://doi.org/10.5194/angeo-2020-68
Preprint. Discussion started: 17 February 2021

Annales Geophysicae Discussions
Open Access
EGU

in the amplitude and phase of the VLF signal. This is illustrated in Fig. 2 (a and b) where the electron density is plotted at z = 85 km as function of x distance and at three different times. For example, the electron density at ($\Delta t_1 = -01:24:33$) has two spatial regions where it exceeds 30.74 cm^{-3} and a region where it decreases much more below its proper ambient value. At ($\Delta t_2 = 00:00:00$) even if the electron density shows a structure of double peaks, it remains higher than 30.74 cm^{-3} inside the sensitive zone. This means that during the passage of the neutral disturbance by the sensitive zone, the reflection height of the VLF signal varies and sometimes moves upward and sometimes downward. Effectively, Fig. 3(a) shows the altitudes at which $n_e(z)$ = 30.74 cm^{-3} as function of time and at the crossing point between the disturbance path and the VLF signal GCP i.e. at x = 1000 km and y = 2000 km. From the plot, H' oscillates between higher altitude (90 km) and lower altitude (83 km) during the passage of the perturbation by the GCP. We also see that H' shows a wavy structure with different periods. Effectively, at the beginning the wave period was around 1h then it becomes lower when the disturbance arrives to the sensitive zone and finally it increases when the storm moves away from the GCP. This is also observed in the spatial variation of H' along the y axis and at three different times, see Fig. 3(b). The moving up of the reference height H' during thunderstorm was also reported by Marshall (2012) and Kotovsky and Moor (2016). Although the mechanisms are not similar but our results also highlight such behavior.

The LWPC simulation of the VLF signal amplitude and phase as function of time due to the neutral atmosphere disturbance and at two difference distances from the transmitter are given in the Fig. 4(a and b). In this simulation we supposed that the disturbance is located at the crossing point between the disturbance axis and the GCP path and that H' values were obtained from GPI simulation results presented in Fig. 3.The results showed clearly the effect of the disturbance on the VLF signal where clear perturbations in the amplitude and the phase were observed with period of several minutes. We also noticed that the perturbation amplitude at 3000 km from the transmitter is sometimes positive and sometimes negative unlike the observed amplitude at 5000 km where it is mostly negative. This is also observed in the spatial plots of the amplitude and phase presented in Fig. 5 where it shows clearly that the received signal perturbation strongly depends on receiver location. This difference is due to the modal composition of the propagating VLF signal as described by (NaitAmor et al., 2016).

4 Discussion and conclusion

In this numerical simulation, we studied the effect of the GW on the D-region ionisation and the propagation of the VLF signal. The numerical results showed that at a fixed altitude, the electron density increases when the neutral density decreases and decreases when the neutral density increases. This is explained by the balance between the production of electrons and loss terms. Indeed, in normal atmosphere the parameters described in the GPI differential equations model decrease with increasing altitude since they are proportional to the neutral density. Thus, under perturbed atmosphere due to GW, these parameters vary similarly to the neutral density where they increase when the neutral density increases and decrease when the neutral density decreases. In opposite manner, the electron density decreases when the loss terms increase and increases when the loss terms decrease. This leads to the moving up of the reference height H' of the VLF signal when the neutral density increases and vice-versa. We also noticed that the time variation of H' shows a wavy structure with different periods depending on the disturbance distance to the sensitive zone of the GCP. After the determination of the new reference height values at different times, we were able to simulate the time variation of the VLF signal amplitude and phase by the use of the LWPC code. Therefore and depending on the distance between the disturbance location and the receiver, the perturbation in the signal amplitude sometimes appears above the ambient signal and sometimes below it at shorter distances and mostly below it at longer distances. This difference in the sign of the signal perturbation amplitude is related to the modal composition of the signal at the disturbance region and the receiver location.

author contributions:

S. NaitAmor: Conceptualization, Methodology, Code correction and paper correction.
A. Benchafaa: code writing and draft paper writing.
G. Mebarki: Software and draft paper writing.

Competing interests: The authors declare that they have no conflict of interest.

https://doi.org/10.5194/angeo-2020-68
Preprint. Discussion started: 17 February 2021

Annales Geophysicae Discussions
Open Access
EGU

References

Brissaud, Q., Martin, R., Garcia, R. F., and Komatitsch, D.: Finite-difference numerical modelling of gravitoacoustic wave propagation in a windy and attenuating atmosphere. Geophysical Journal International, 206(1), 308–327. https://doi.org/10.1093/gji/ggw121, 2016.

Dhaka, S. K., Takahash. I. M., Shibagaki. Y., Yamanaka. M. D., and Fukao, S.: Gravity wave generation in the lower stratosphere due to passage of the typhoon 9426 (Orchid) observed by the MU radar at Shigaraki (34.85°N, 136.10°E), J. Geophys. Res., 108, D19, 4595, DOI:10.1029/2003JD003489, 2003.

Ding, F., Wan, W., and Yuan, H.: The influence of background winds and attenuation on the propagation of atmospheric gravity waves, J. Atmos. Sol.-Terr. Phys., 65(7), 857–869, 2003.

Ferguson, J. A.: Computer Programs for Assessment of Long-Wavelength Radio Communications, Version 2.0: User's Guide and Source Files, No. TD-3030, Space and Naval Warfare Systems Center, San Diego CA, 1998.

Glukhov, V. S., Pasko. V. P., and Inan, U. S.: Relaxation of transient lower ionospheric disturbances caused by lightning-whistler-induced electron precipitation bursts,J. Geophys. Res., 97, 16,971 – 16,979, 1992.

Graves, R.W.: Simulating seismic wave propagation in 3D elastic media using staggered-grid finite differences, Bull. seism. Soc. Am.,86(4),1091–1106, 1996.

Haldoupis, C., Mika. Á., and Shalimov, S.: Modeling the relaxation of early VLF perturbations associated with transient luminous events, J. Geophys. Res. Sp. Phys., 114(A00E04), doi:10.1029/2009JA014313, 2009.

Hedin, A. E.: Extension of the MSIS thermospheric model into the middle and lower atmosphere,J. Geophys. Res., 96(A2),1159–1172, doi:10.1029/90JA02125, 1991.

Ibrahim, C., Barthe. C., Jolivet. S., Keckhut, P., Liou. Y.-A., and Kuleshov, Y.: Observation and a numerical study of gravity waves during tropical cyclone Ivan (2008), Atmos. Chem. Phys., 14, 641–658, DOI:10.5194/acp-14-641-2014, 2014.

Inan, U. S., Cummer, S. A., and Marshall, R. A.: A Survey of ELF and VLF Research 289. On Lightning−Ionosphere Interactions and Causative Discharges, J. Geophys. Res. Space 290. Physics, 115, A00E36, Doi:10.1029/2009JA014775, 2010.

Jean-Pierre Raulin., Grard Trottet., Matthieu Kretzschmar., Edith Macotela., Alessandra Pacini., et Al..: Response Of The Low Ionosphere To X-Ray And Lyman-α Solar Flare Emissions. Journal Of Geophysical Research: Space Physics, American Union/Wiley, 118, Pp.570-575. Doi:10.1029/2012JA017916. Insu-01179432, 2013.

Kumar, S., NaitAmor, S., Chanrion, O., and Neubert, T.: Perturbations to the lower ionosphere by tropical cyclone Evan in the South Pacific Region. Journal of Geophysical Research: Space Physics, 122, 8720–732. https://doi.org/10.1002/2017JA024023, 2017.

Kumar, S., Kumar. A., Menk. F., Maurya. A. K., R. Singh., and Veenadhari, B.: Response Of The Low-Latitude D Region Ionosphere To Extreme SpaceWeather Event Of 1416 December 2006, J. Geophys. Res. Space Physics, 120, 788799, Doi: 10.1002/2014JA020751, 2015.

Le Pichon, A., Blanc, E. and Hauchecorne, A.: Infrasound Monitoring for Atmospheric Studies, Springer, 2010.

Marshall, R. A., and Snively, J. B.: Very low frequency subionospheric remote sensing of thunderstorm-driven acoustic waves in the lower ionosphere, J. Geophys. Res.,119, DOI: 10.1002/2014JD0215940, 2014.

Moore, R. C., Barrington-Leigh, C. P., Inan, U. S. and Bell., T. F.: Early/fast VLF events produced by electron density changes associated with sprite halos, J. Geophys. Res., 108(A10), 1363, doi:10.1029/2002JA009816, 2003.

https://doi.org/10.5194/angeo-2020-68
Preprint. Discussion started: 17 February 2021

Naitamor, S., Alabdoadaim, M. A., Cohen, M. B., Cotts, B. R. T., Soula, S., Chanrion, O., Neubert, T., and Abdelatif, T.: VLF Observations Of Ionospheric Disturbances In Association With TLEs From The Eurosprite 2007 Campaign, J. Geophys. Res., 115, A00E47, Doi:10.1029/2009JA015026, 2010.

NaitAmor, S., Cohen, M. B., Kumar, S., Chanrion, O., and Neubert, T.: VLF signal anomalies during cyclone activity in the Atlantic Ocean.Geophysical Research Letters, 45, 10,185–10,192. https://doi.org/10.1029/2018GL078988, 2018.

NaitAmor, S., Ghalila. H., and Cohen, M. B.: TLEs and early VLF events: Simulating the important impact of transmitter-disturbance-receiver geometry, J. Geophys. Res., 121, 792-801, DOI: 10.1002/2016JA022791, 2016.

Nina, A., and Čadež, V. M.: Detection of acoustic-gravity waves in lower ionosphere by VLF radio waves, Geophys. Res., Lett., 40, 4803–4807, DOI:10.1002/grl.50931, 2013.

Ming, F., Ibrahim, C., Barthe, C., C., Jolivet, S., Keckhut, P., Liou, Y.-A., and Kuleshov, Y.: Observation and a numerical study of gravity waves during tropical cyclone Ivan (2008).Atmospheric Chemistry and Physics, 14, 641–658. https://doi.org/10.5194/acp-14-641-2014, 2014.

Occhipinti, G., Coïsson, P., Makela, J. J., Allgeyer, S., Kherani, A., Hébert, H., and Lognonne, P.: Three-dimensional numerical modeling of tsunami-related internal gravity waves in the Hawaiian atmosphere, Earth Planet. Sci., 63, 847–851, doi:10.5047/eps.2011.06.051, 2011.

Pal, S., Chakraborty, S., and Chakrabarti, S. K.: On the use of Very Low Frequency transmitter data for remote sensing of atmospheric gravity and planetary waves, Adv. Sp. Res., 55(4), 1190– 1198, 2015.

Palit, S., Basak, T., Pal, S., Mondal, S. K., and Chakrabarti, S. K.: "Effect of solar flares on ionospheric VLF radio wave propagation, modeling with GEANT4 and LWPC and determination of effective reflection height," 2014 XXXIth URSI General Assembly and Scientific Symposium (URSI GASS), Beijing, pp. 1-4, doi: 10.1109/URSIGASS.2014.6929558, 2014.

Perevalova, N. P., and Ishin, A. B.: Effects of Tropical Cyclones in the Ionosphere from data of sounding by GPS Signals, Atmos. and Oceanic Phys., 47, 1072–1083, DOI: 10.1134/S000143381109012X, 2011.

Rozhnoi, A., Solovieva, M., Levin, B., Hayakawa, M., and Fedun, V.: Meteorological effects in the lower ionosphere as based on VLF/LF signal observations, Nat. Hazards Earth Syst. Sci., 14, 2671–2679, DOI:10.5194/nhessd-2-2789-2014.

Song, Q., Ding, F., Zhang, X., and Mao, T.: GPS detection of the ionospheric disturbances over China due to impacts of Typhoons Rammasum and Matmo, J. Geophys. Res. Space Physics, 122, 1055–1063, DOI:10.1002/2016JA023449, 2017.

Velinov, P., Asenovski, S., Kudela, K., Lastovicka, J., Mateev, L., et al..: Impact of cosmic rays and solar energetic particles on the Earth's ionosphere and atmosphere. J. Space Weather Space Clim.,3, A14, 2013.

Wait, J. R., and Spies, K. P.: Characteristics of the Earth-ionosphere waveguide for VLF radio waves, Tech. Note 300, Natl. Bur. of Stand., Boulder, Co, 1964.

https://doi.org/10.5194/angeo-2020-68
Preprint. Discussion started: 17 February 2021

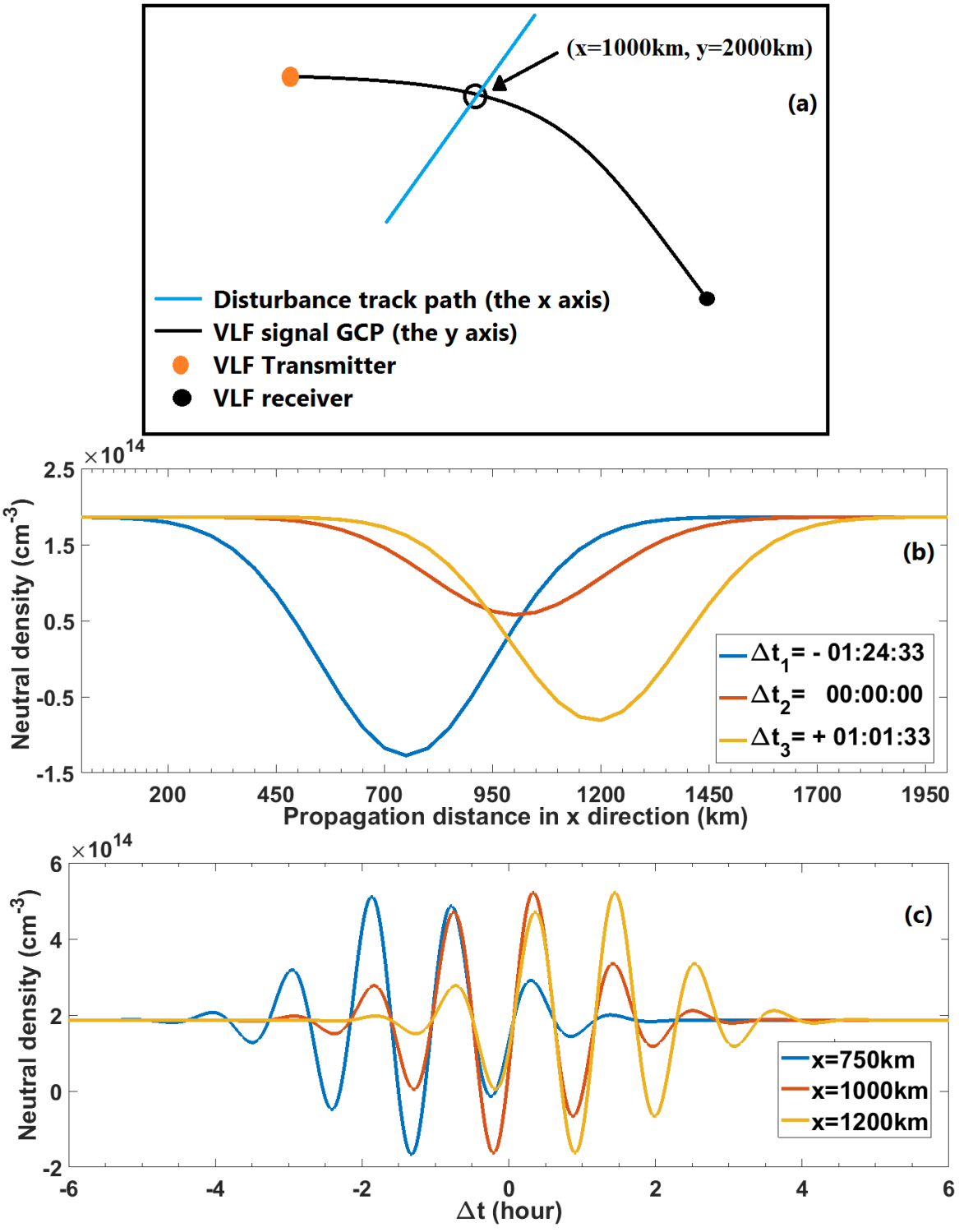

Figure 1: a) Geometry of the simulations. b) Spatial variation of the neutral density. c) Temporal variation of the neutral density.

https://doi.org/10.5194/angeo-2020-68
Preprint. Discussion started: 17 February 2021

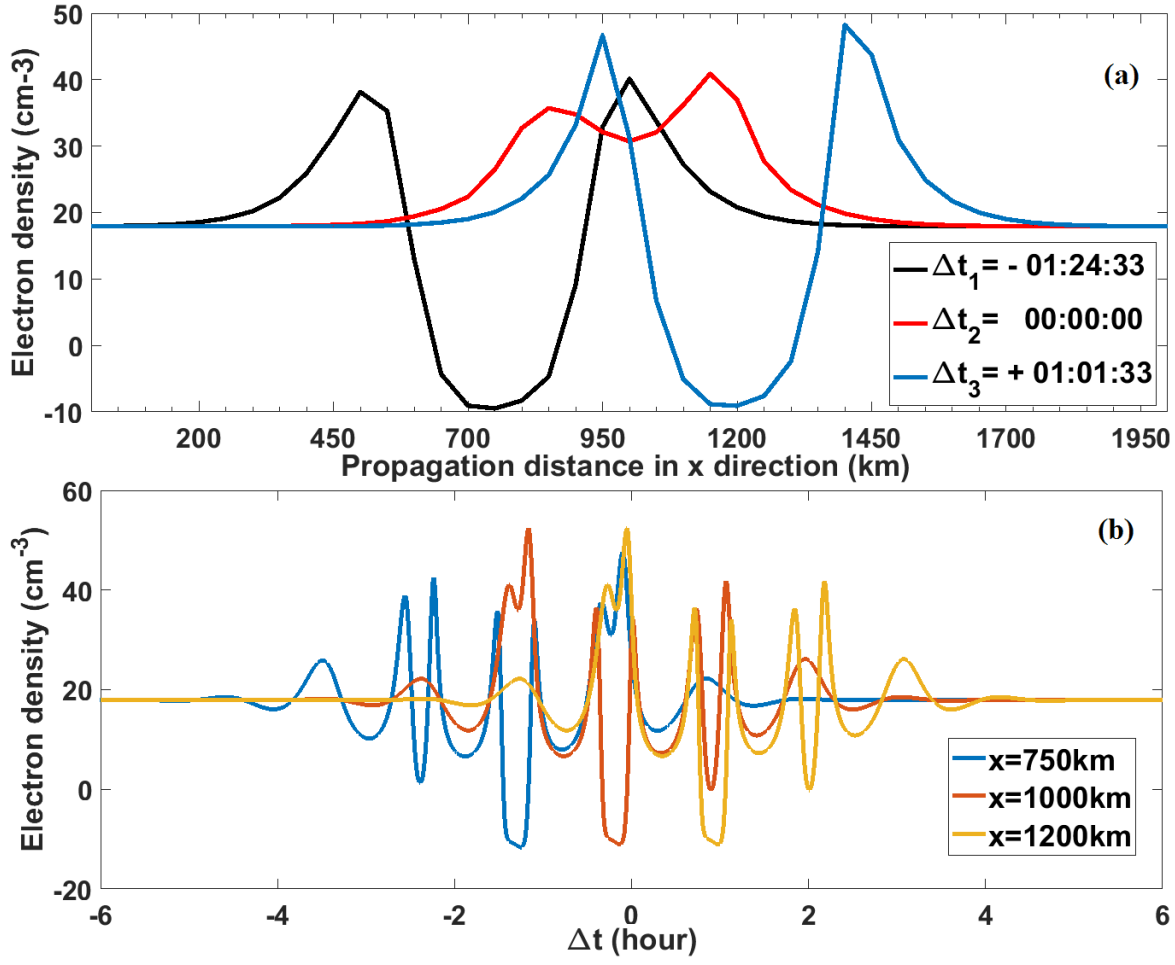

Figure 2: (a): electrons density as a function of distance at z = 85 km at different instants, (b): electrons density as a function of the time at different positions.

https://doi.org/10.5194/angeo-2020-68
Preprint. Discussion started: 17 February 2021

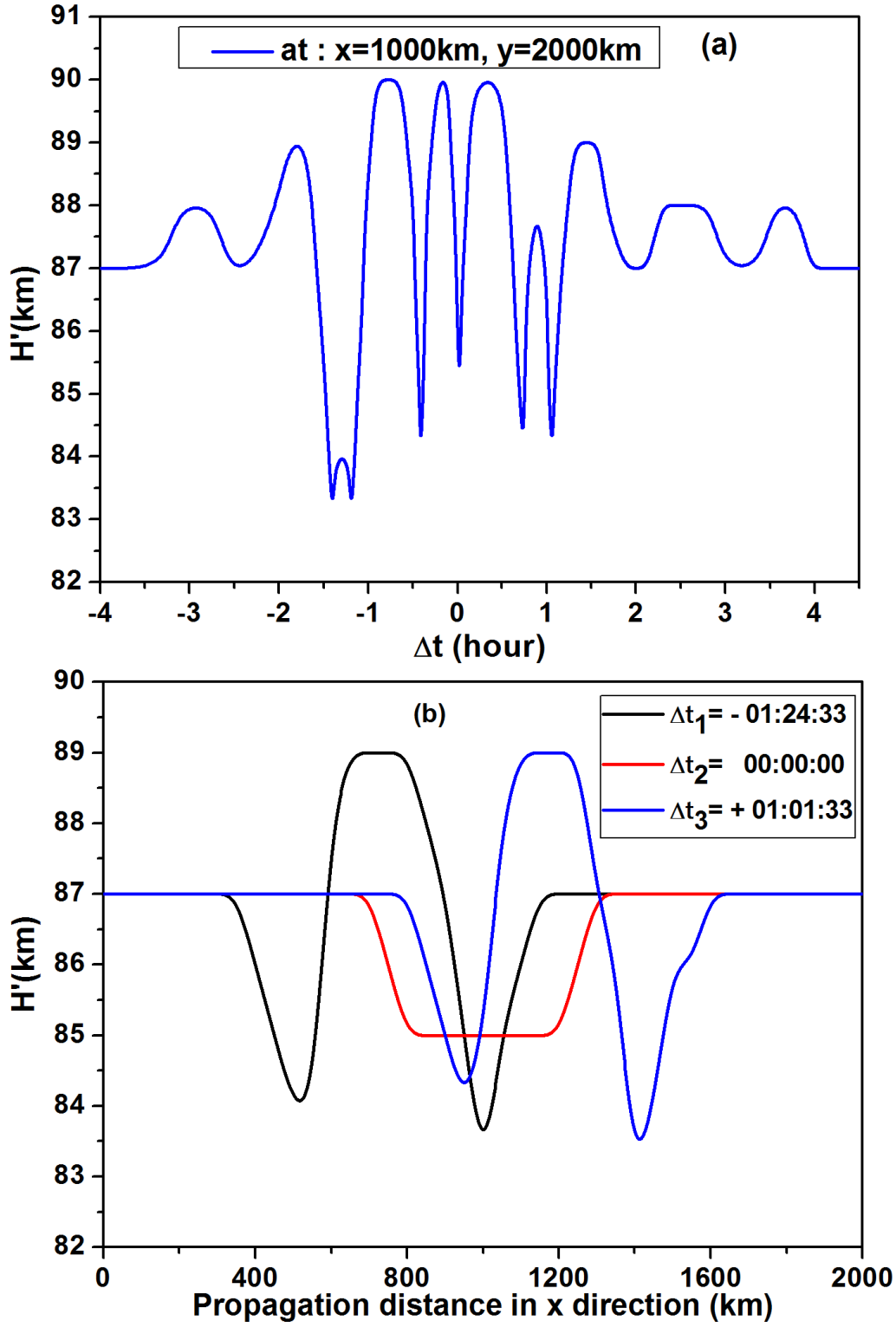

Figure 3: (a) the Wait parameter (H′) as a function of the time at the position y = 2000 km, x =1000 km, (b): the Wait parameter (H′) as a function of distance at y=2000km and at different instants.

https://doi.org/10.5194/angeo-2020-68
Preprint. Discussion started: 17 February 2021

Annales Geophysicae Discussions
Open Access
EGU

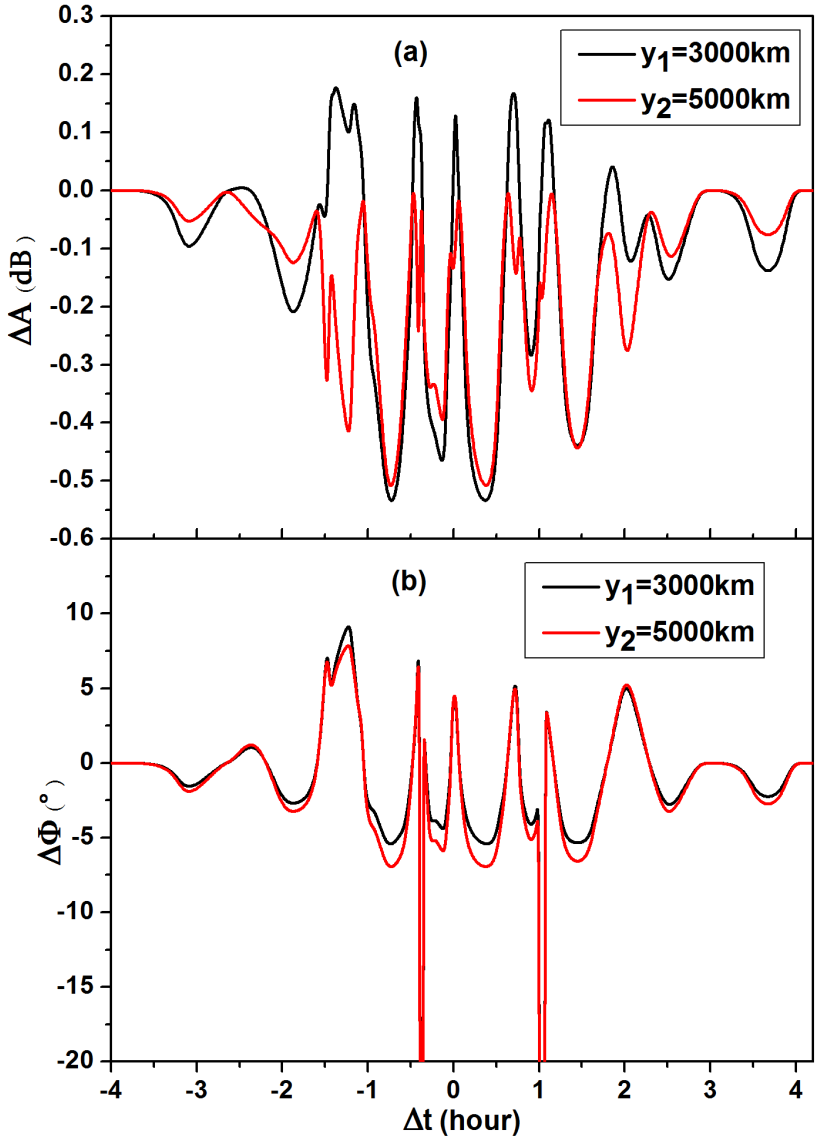

Figure 4: (a) the difference of the amplitude as a function of the time at two positions, (b): the difference of the phase as a function of the time at two positions: $y_1 = 3000km$, $y_2 = 5000km$.

https://doi.org/10.5194/angeo-2020-68
Preprint. Discussion started: 17 February 2021

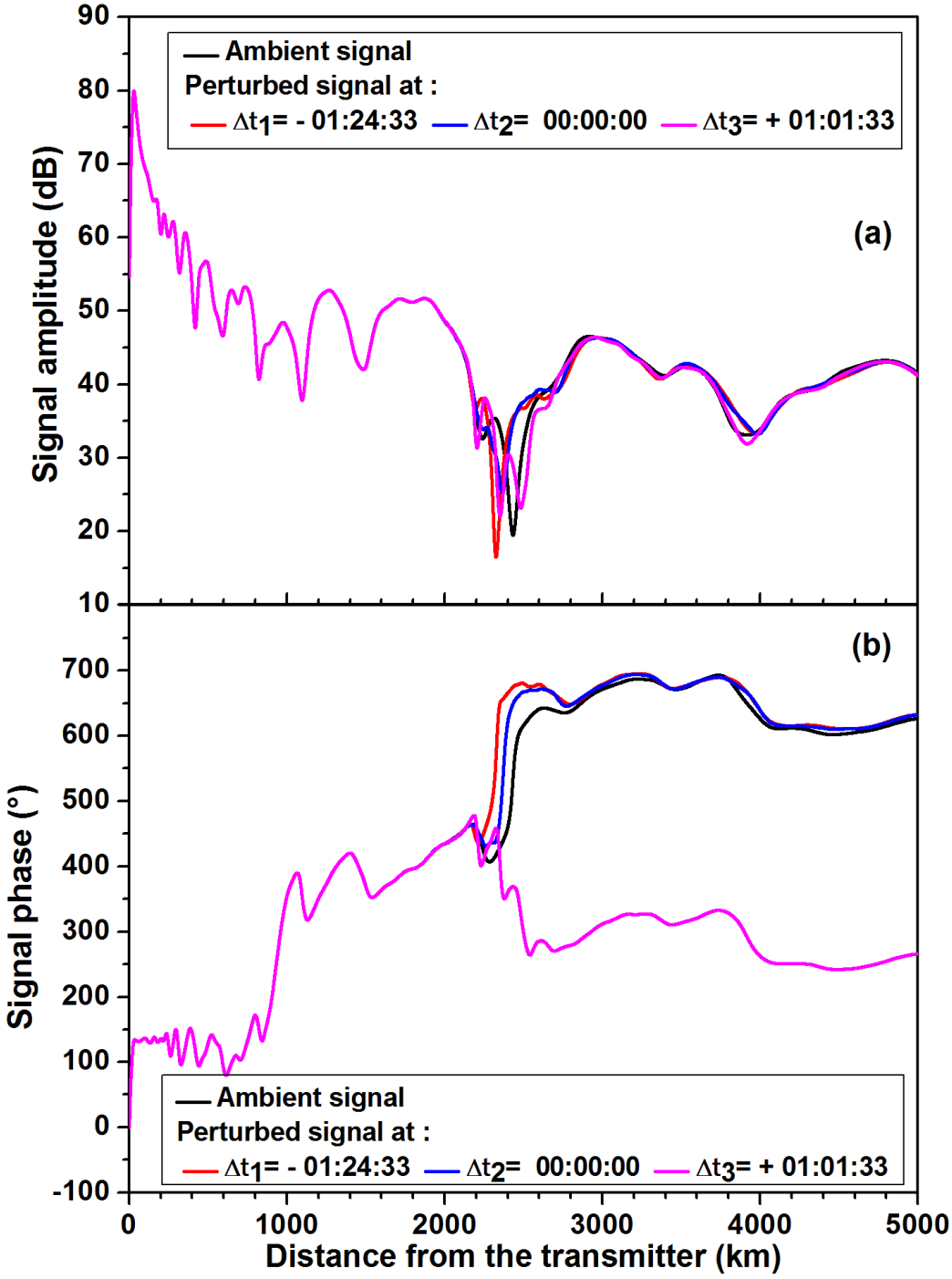

Figure 5: (a) the Amplitude as a function of the distance from the transmitter at the ambient and at the different instants. (b): the phase as a function of the distance from the transmitter at the ambient and at the same instants.